© 2023. Published by The Company of Biologists Ltd | Development (2023) 150, dev202115. doi:10.1242/dev.202115

RESEARCH ARTICLE

Actin and CDC-42 contribute to nuclear migration through constricted spaces in *C. elegans*

Jamie Ho[1], Leslie A. Guerrero[1], Diana E. Libuda[2], G. W. Gant Luxton[1] and Daniel A. Starr[1,*]

ABSTRACT

Successful nuclear migration through constricted spaces between cells or in the extracellular matrix relies on the ability of the nucleus to deform. Little is known about how this takes place *in vivo*. We have studied confined nuclear migration in *Caenorhabditis elegans* larval P cells, which is mediated by the LINC complex to pull nuclei towards the minus ends of microtubules. Null mutations of the LINC component *unc-84* lead to a temperature-dependent phenotype, suggesting a parallel pathway for P-cell nuclear migration. A forward genetic screen for enhancers of *unc-84* identified *cgef-1* (CDC-42 guanine nucleotide exchange factor). Knockdown of CDC-42 in the absence of the LINC complex led to a P-cell nuclear migration defect. Expression of constitutively active CDC-42 partially rescued nuclear migration in *cgef-1; unc-84* double mutants, suggesting that CDC-42 functions downstream of CGEF-1. The Arp2/3 complex and non-muscle myosin II (NMY-2) were also found to function parallel to the LINC pathway. In our model, CGEF-1 activates CDC-42, which induces actin polymerization through the Arp2/3 complex to deform the nucleus during nuclear migration, and NMY-2 helps to push the nucleus through confined spaces.

KEY WORDS: Cdc42, LINC, Actin networks, Nuclear envelope, Nuclear migration

INTRODUCTION

Cellular migration through constricted spaces is a process that occurs during the immune response, tissue development and cancer metastasis (Bone and Starr, 2016; Denais et al., 2016; Thiam et al., 2016). During mammalian brain development, newly born neurons must migrate from the germinal layers to the developing cortices by migrating through constrictions generated by the surrounding neural tissue (Kalukula et al., 2022; Kengaku, 2018). Additionally, during the immune response, neutrophils in the bloodstream must migrate through the endothelial monolayer of the blood vessels in order to access the site of inflammation or tissue injury (Liu et al., 2021; Salvermoser et al., 2018). The rate of cellular migration through narrow spaces is limited by nuclear deformability, as the nucleus is the largest and most rigid organelle of the cell (Friedl et al., 2011; Fu et al., 2012; Swift et al., 2013; Wolf et al., 2013). Nuclear deformability is dependent on several factors, such as lamin composition, levels of heterochromatin and cytoskeletal dynamics. Low expression or knockdown of laminA and/or laminC, or low levels of heterochromatin result in increased nuclear deformability (Bell et al., 2022; Davidson et al., 2014; 2015; Stephens et al., 2018). Additionally, cytoskeletal forces applied to nuclei can affect nuclear deformability (Renkawitz et al., 2019; Thiam et al., 2016). Mouse dendritic cells that are induced to migrate through constrictions are unable to undergo successful nuclear migration when the actin-nucleating Arp2/3 complex is inhibited (Thiam et al., 2016), highlighting the importance of actin during this process. In addition, nuclear migration through constricted spaces leads to nuclear envelope rupture and increased DNA damage (Denais et al., 2016; Raab et al., 2016; Thiam et al., 2016). Most of these findings were made using *in vitro* systems of cells migrating through manufactured constricted spaces. A system where mouse dendritic cells are imaged migrating through the extracellular matrix of explanted mouse ears has been used to find more *in vivo* relevance (Raab et al., 2016). However, how cells and nuclei migrate through constricted spaces as a normal part of development *in vivo* is poorly understood.

We developed an *in vivo* model to study nuclear migration through constricted spaces using larval hypodermal precursor cells (P cells) in *C. elegans* (Fig. 1A) (Bone et al., 2016; Chang et al., 2013). During the early L1 larval stage, 12 P cells organized into six pairs span the lateral side to the ventral side of the animal, with the nuclei located on the lateral side of the animal (Sulston and Horvitz, 1977). During mid-L1 development, P-cell nuclei, which are 3-4 µm in diameter, migrate from their lateral positions to the ventral cord by squeezing through a narrow space of ∼200 nm between the body wall muscles and the cuticle (Bone et al., 2016; Cox and Hardin, 2004; Francis and Waterston, 1991). This constriction is about 5% of the diameter of the nucleus. After P-cell nuclei successfully migrate, they divide and develop into vulval cells and GABA neurons. Failed nuclear migration results in P-cell death, which results in the lack of a vulva and GABA neurons, leading to egg laying-deficient (Egl) and uncoordinated (Unc) phenotypes (Horvitz and Sulston, 1980; Sulston and Horvitz, 1981). The P-cell death observed in *unc-84(null)* mutants is morphologically distinct from normal programmed cell death and are not affected by the *ced-3(n717)* mutation (Malone et al., 1999).

P-cell nuclear migration is regulated by the SUN (Sad1 and UNC-84) protein UNC-84 and the KASH (Klarsicht, ANC-1, Syne homology) protein UNC-83 (Malone et al., 1999; Starr et al., 2001). UNC-84, which is located at the inner nuclear membrane, interacts with UNC-83 to recruit it to the outer nuclear membrane (McGee et al., 2006). Together, UNC-84 and UNC-83 form a LINC (linker of nucleoskeleton and cytoskeleton) complex to transfer forces generated by the cytoskeleton in the cytoplasm to structures inside the nucleus (Starr and Fridolfsson, 2010). UNC-83 is then able to interact with microtubule motor proteins kinesin 1 and cytoplasmic

[1]Department of Molecular and Cellular Biology, University of California, Davis, CA 95616, USA. [2]Department of Biology, University of Oregon, Eugene, OR 97403, USA.

*Author for correspondence (dastarr@ucdavis.edu)

D.E.L., 0000-0002-4944-1814; G.W.G.L., 0000-0002-6180-8906; D.A.S., 0000-0001-7339-6606

Handling Editor: Swathi Arur
Received 22 June 2023; Accepted 15 September 2023

Development (2023) 150, dev202115. doi:10.1242/dev.202115

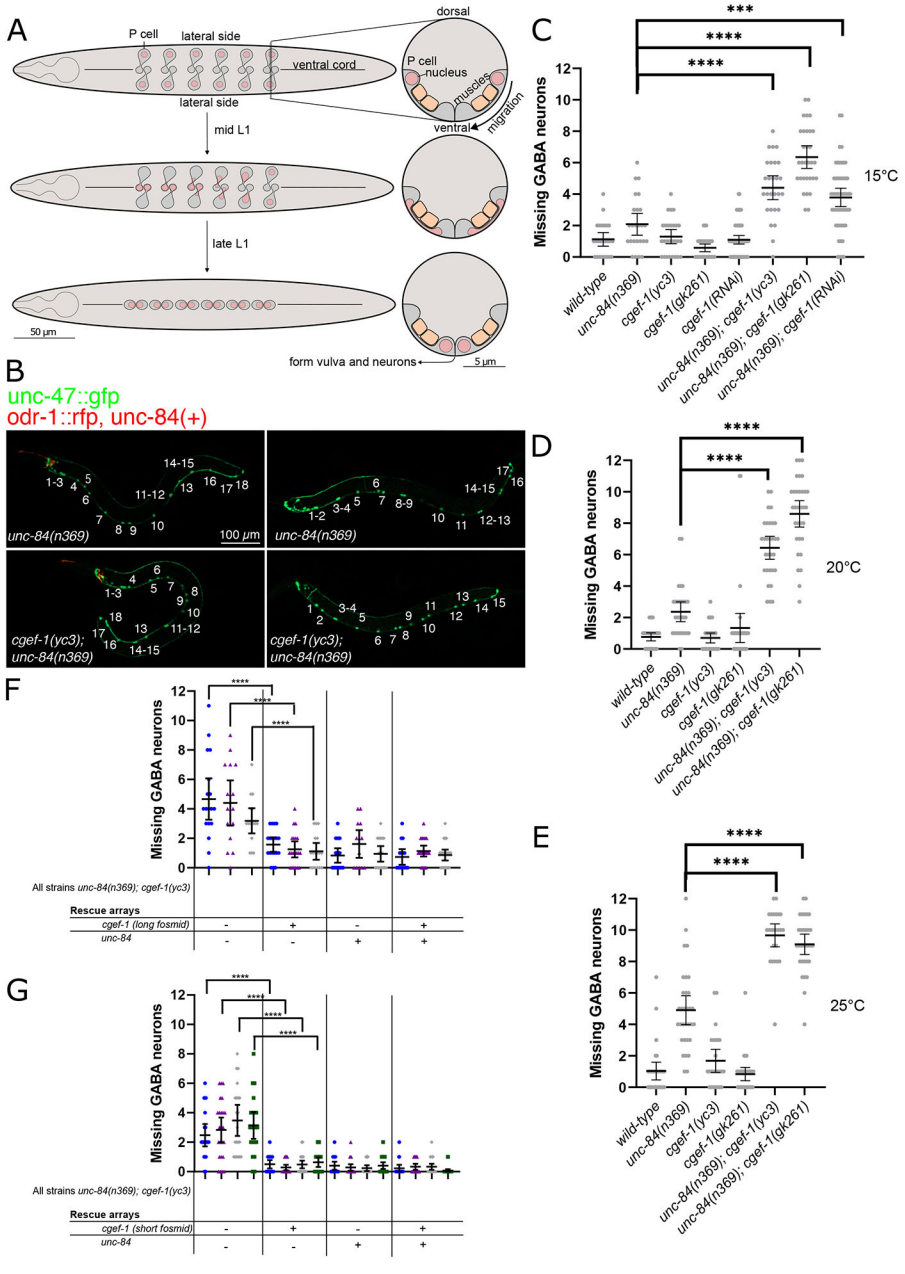

Fig. 1. Mutations in *cgef-1* enhance the P-cell nuclear migration defect of *unc-84(null)*. (A) Schematic of P-cell nuclear migration. (Left) Ventral views of L1 larva during P-cell nuclear migration. Anterior is towards the left, where a pharynx is drawn. The ventral cord is marked with a line down the center of the larvae. (Right) Cross-sections of analogous stages with the ventral surface of the animal facing down. (Top) Before the onset of P-cell nuclear migration, P cells (gray) span from the lateral to the ventral side of the worm, with the nuclei (pink circles) located laterally. The P cell is partitioned into a lateral and ventral region by a narrow constriction between body wall muscles (orange in cross-section) and the cuticle. (Middle) When nuclear migration begins, P-cell nuclei migrate through the constriction towards the ventral region. This process starts with the most anterior pair of P cells and is followed by the consecutive pairs. (Bottom) P-cell nuclear migration ends when all 12 nuclei have migrated to the ventral cord. (B) Representative epifluorescence images of L4 animals expressing *unc-47::gfp* in ventral cord GABA neurons in *unc-84(n369)* (top panels) and *unc-84(n369, cgef-1(yc3)* double mutants (bottom panels). Animals expressing an *unc-84(+)* rescue array also express *odr-1::rfp* in the head (left panels). L4 larvae are shown from the lateral side with anterior towards the left and ventral down. (C-E) Plots of the number of missing GABA neurons at 15°C (C), 20°C (D) and 25°C (E) of the *unc-84(n369)*, *oxIs12(unc-47::gfp); ycEx60(odr-1::rfp,WRM0617cH07)* and *cgef-1(yc3)* single and double mutants. (F) Plot of the number of missing GABA neurons when both *WRM0625dG08* and *WRM0622bA03* fosmids (long fosmids) are expressed at 15°C. Each color represents an independent line with a total of three independent lines assayed for P-cell nuclear migration defects. (G) Number of missing GABA neurons when *WRM0627cD01* fosmid (short fosmid) is expressed at 15°C. Each color represents an independent line with a total of four independent lines assayed for P-cell nuclear migration defects. OE indicates overexpression of the indicated transgene. All error bars are 95% confidence intervals. For C-E, statistical analyses were carried out using one-way ANOVA with Holm-Sidak's corrections for multiple comparisons. ***P<0.001, ****P<0.0001.

dynein to move nuclei (Fridolfsson et al., 2010; Fridolfsson and Starr, 2010; Meyerzon et al., 2009). In larval P-cells, dynein is the major motor that functions to move nuclei toward the minus ends of microtubules in the ventral cord (Bone et al., 2016; Ho et al., 2018). Null mutations in *unc-83* or *unc-84* lead to a temperature-sensitive nuclear migration defect in P cells. When these mutants are grown at 25°C, less than 40% of P-cell nuclei successfully migrate to a ventral position. However, when the LINC complex is disrupted at 15°C, at least 90% of P-cell nuclei migrate successfully (Malone et al., 1999; Starr et al., 2001). This leads to our hypothesis that there is an additional pathway that functions parallel to the LINC complex-dependent pathway to move P-cell nuclei through constricted spaces.

To identify players in this alternative nuclear migration pathway, we have previously conducted an unbiased forward genetics screen for enhancers of the nuclear migration defect of *unc-84* (*emu*) at 15°C (Chang et al., 2013). Eight *emu* mutations were isolated in these screens and one was identified as a lesion in *toca-1* (transducer of Cdc-42-dependent actin assembly) (Chang et al., 2013). TOCA-1 is predicted to have a F-BAR domain, a domain that interacts with the Rho GTPase Cdc42 and a domain that interacts with actin-nucleating WASP proteins (Fricke et al., 2009; Giuliani et al., 2009; Ho et al., 2004). One model proposed that TOCA-1 functions by binding to the nuclear membrane, recruiting Cdc42 and WASP to nucleate actin, and deforming the nucleus to aid in migration. There is an extensive, but poorly defined, actin network in larval P cells (Bone et al., 2016).

Here, we report the identification of a second *emu* allele in *cgef-1* that is predicted to encode a guanine nucleotide exchange factor (GEF) for CDC-42 (Chan and Nance, 2013). GEFs function by

Development (2023) 150, dev202115. doi:10.1242/dev.202115

activating G proteins, which are molecular switches involved in regulating signaling cascades. G-proteins can be found in an 'inactive' GDP-bound state and an 'active' GTP-bound state. GEFs activate G-proteins by facilitating the exchange of GDP for GTP (Rossman et al., 2005; Schmidt and Hall, 2002). The Rho-GTPase family of G-proteins includes RhoA, Rac and Cdc42, which function by regulating polarity establishment, cell movement and cytoskeletal dynamics (Etienne-Manneville, 2004; Hall, 1998). *C. elegans* orthologs are RHO-1, CED-10 (Rac), MIG-2 (Rac) and CDC-42 (Reiner and Lundquist, 2018). CGEF-1 acts as a GEF for CDC-42 during early embryonic development (Chan and Nance, 2013), but its role outside embryogenesis is unclear. We propose that CGEF-1 activates CDC-42, which then assembles actin networks to help nuclei migrate through constricted spaces in a pathway that functions parallel to the LINC complex and dynein pathway. To test this hypothesis, we examined the roles of CGEF-1, CDC-42 and other actin regulators during P-cell nuclear migration.

RESULTS

Mutations in *cgef-1* enhance the P-cell nuclear migration defect of *unc-84(null)* animals

The *yc3* and *yc21* alleles were found in an *emu* screen and the homozygous mutants significantly enhance the nuclear migration defect of *unc-84* (Chang et al., 2013). To quantify P-cell nuclear migration, we expressed the GABA neuronal marker $p_{unc\text{-}47}$*::gfp* and counted the number of GABA neurons at the L4 stage as an indicator of successful P-cell nuclear migration (Fridolfsson et al., 2018; McIntire et al., 1997). At 15°C, *unc-84(n369)* mutants were missing an average of 2.08±0.66 [mean±95% confidence interval (CI)] GABA neurons, slightly above wild type (Fig. 1B,C). *yc3* single mutants had no phenotype on their own, missing an average of 1.30±0.43 GABA neurons. However, *yc3, unc-84(n369)* double mutants had an average of 4.41±0.73 missing GABA neurons (P<0.00005). *yc3* also enhanced the nuclear migration defect of *unc-84(n369)* at 20°C and at 25°C (Fig. 1D,E).

To identify the molecular lesion underlying *emu* alleles, we performed whole-genome sequencing of seven different *emu* mutant strains isolated in our previous screen (Chang et al., 2013). We cataloged single nucleotide polymorphisms (SNPs) that were predicted to cause severe disruptions to open reading frames. SNPs that were found in all the strains were eliminated because they were likely in the background of the UD87 strain that was used for mutagenesis. We focused on a SNP predicted to cause a premature stop codon in the *cgef-1* gene that was identified in both the *yc3* and *yc21* alleles. Nucleotide X:2798063 in the penultimate exon of *cgef-1* was mutated from a G to an A, causing the tryptophan 345 of CGEF-1a to change to a premature stop codon (Fig. 2A).

To confirm that the premature stop codon in *cgef-1(yc3)* is the molecular lesion responsible for enhancing the nuclear migration defect of *unc-84*, we tested whether other alleles of *cgef-1* also enhance the P-cell nuclear migration defect of *unc-84(n369)* null mutants. *cgef-1(gk261)* is likely a null allele, as it is a 318 bp deletion that removes the entire third exon in *cgef-1a* and is predicted to result in a frame shift (Fig. 2A) (*C. elegans* Deletion Mutant Consortium, 2012). *cgef-1(gk261) unc-84(n369)* double mutants had significant P-cell nuclear migration defects at 15°C, 20°C and 25°C compared with the single mutants (Fig. 1C-E). Likewise, *cgef-1(RNAi)* significantly enhanced the nuclear migration defects of *unc-84(n369)* (Fig. 1C-E). Thus, multiple alleles and RNAi of *cgef-1* all had similar phenotypes.

To confirm that the *yc3* phenotype is due to the molecular lesion in *cgef-1* and not some other mutation in the genome, we expressed *cgef-1* extra-chromosomal rescue arrays in *yc3, unc-84(n369)* double mutants. Two fosmids that together cover the longest predicted isoforms of *cgef-1* (WRM0622bA03 and WRM0625dG08) were able to rescue the nuclear migration defect in three independent lines (P<0.0005) (Fig. 1F). Together, these data strongly suggest that lesions in *cgef-1* are responsible for the nuclear migration defects observed in *yc3* and *yc21* animals, and that *cgef-1* functions in parallel with the LINC complex to facilitate P-cell nuclear migration.

The *cgef-1d* isoform functions in P-cell nuclear migration

CGEF-1 activates CDC-42 during early embryogenesis (Chan and Nance, 2013; Kumfer et al., 2010). *C. elegans* encodes at least four *cgef-1* predicted isoforms (Fig. 2A) (Ziel et al., 2009; Wormbase). All four isoforms share the last four exons of the *cgef-1* gene, which are predicted to encode a catalytic Dbl homology (DH) domain, as well as a pleckstrin homology (PH) domain (Chan and Nance, 2013; Ziel et al., 2009). *cgef-1a* and *cgef-1c* encode the shortest CGEF-1 isoforms that differ in length by only two amino acids at their N termini. *cgef-1b* encodes the longest CGEF-1 isoform, whereas *cgef-1d* encodes an isoform that is intermediate in length. Expression of a fosmid (WRM0627cD01) that spans only the *cgef-1a*, *cgef-1c* and *cgef-1d* isoforms was sufficient to rescue the *cgef-1(yc3) unc-84* nuclear migration defect at 15°C, indicating that exons 1-11 of *cgef-1b* are not necessary for P-cell nuclear migration (Fig. 1G).

To further determine which isoform of *cgef-1* functions in this process, we generated new alleles in each isoform using CRISPR-Cas9 gene editing, either as an early stop codon in the first or second exon of an isoform or as a deletion mutation that resulted in a predicted frameshift (Fig. 2A). Predicted severe alleles of the long isoforms, *cgef-1b(yc101)* and *cgef-1b(yc102)*, did not enhance the nuclear migration defect of *unc-84(n369)* at 15 or 20°C (Fig. 2B,C). In contrast, the *cgef-1d(yc103)* early stop codon and *cgef-1d(yc104)* frame-shift deletion mutations significantly enhanced the nuclear migration defect of *unc-84(n369)* at 15 and 20°C (Fig. 2C). Mutations in the shortest isoforms, *cgef-1a,c(yc109)* and *cgef-1a, c(yc110)*, also enhanced the nuclear migration defect of *unc-84(n369)* at 20°C but not at 15°C. Thus, we conclude that *cgef-1b* is dispensable for P-cell nuclear migration whereas *cgef-1d* and *cgef-1a,c* contribute to nuclear migration when the LINC complex is disrupted.

We next determined whether the *cgef-1a,c* and *cgef-1d* isoforms are expressed in P-cells during nuclear migration. We used previously described 5′*cis*-regulatory element reporter strains that drive the expression of GFP under the control of promoters for *cgef-1d* or *cgef-1a,c* (Ziel et al., 2009) (Fig. 2A), and looked for GFP expression in L1 larval P-cells, which were marked with a tdTomato nuclear marker expressed from the P-cell specific promoter of *hlh-3* (Bone et al., 2016; Chang et al., 2013). The *cgef-1d* reporter expressed GFP in larval P cells. However, the *cgef-1a,c* reporter did not express detectable GFP above background in larval P cells. Thus, *cgef-1d* appears to be the main isoform expressed in P-cells and it functions during nuclear migration in these cells.

CGEF-1 activates CDC-42 during P-cell nuclear migration

As CGEF-1 activates the small GTPase CDC-42 in early embryogenesis (Chan and Nance, 2013; Kumfer et al., 2010), we hypothesized that *cdc-42* is downstream of *cgef-1* and together they help P-cell nuclei migrate in the absence of *unc-84*. To test this, we knocked down *cdc-42* specifically in larval P cells at the time of nuclear migration using the auxin-inducible degradation (AID)

Development (2023) 150, dev202115. doi:10.1242/dev.202115

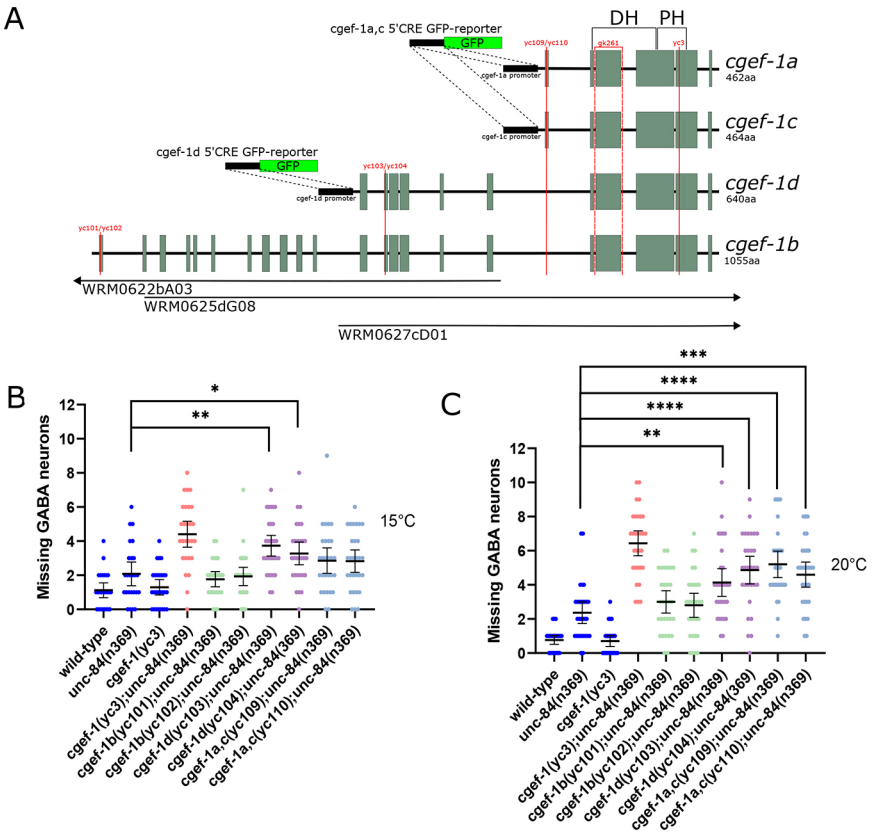

Fig. 2. The *cgef-1d* isoform contributes to P-cell nuclear migration. (A) Intron (black lines) and exon (green boxes) schematics for the four known *cgef-1* isoforms. All isoforms share the same 3′ end, which encodes Dbl homology (DH) and Pleckstrin homology (PH) domains. The red vertical lines that run perpendicular to the diagrams show where the labeled mutations are located. The regions that the *WRM0625dG08*, *WRM0622bA03* and *WRM0627cD01* fosmids overlap are indicated at the bottom and the arrows indicate that the fosmids continue beyond the genomic region shown in the diagram. *cgef-1a,c* and *cgef-1d* 5′*cis*-regulatory element (5′CRE) GFP-reporters are shown. These constructs were generated by using 2.5 kb region upstream of each isoform transcript to drive GFP expression. (B,C) Plot of the number of missing GABA neurons at 15°C (B) and at 20°C (C) of *cgef-1* isoform mutations. (D) Representative images of *phlh-3::nls::tdTomato* (red) and *cgef-1a,c* 5′CRE GFP-reporter (top row) and *cgef-1d* 5′CRE GFP-reporter (bottom row). White arrows indicate areas of colocalization. All error bars are 95% confidence intervals and all statistical analysis was carried out using one-way ANOVA analyses with Holm-Sidak's corrections for multiple comparisons. **P*<0.05, ***P*<0.01, ****P*<0.001, *****P*<0.0001.

system (Ho et al., 2018; Zhang et al., 2015). We tagged the endogenous *cdc-42* locus with a 44-amino acid degron using CRISPR/Cas9 engineering and expressed the TIR-1 E3 ubiquitin ligase under the control of the P-cell specific *hlh-3* promoter. This combination of tissue-specific expression of TIR-1 and the addition of auxin during the mid-L1 larval stage, when P-cell nuclear migration occurs, allowed for spatial and temporal control of CDC-42 protein degradation. We found that degrading CDC-42 in otherwise wild-type L1 larvae had no effect on P-cell nuclear migration (Fig. 3A). However, CDC-42 auxin-induced degradation significantly enhanced the *unc-84(null)* nuclear migration defect at both 15°C and 25°C (Fig. 3A-B), suggesting that CDC-42 contributes to P-cell nuclear migration in the absence of LINC complexes.

We next tested whether *cdc-42* is in the same pathway as *cgef-1* by degrading CDC-42 in *cgef-1, unc-84* double mutants. Degradation of CDC-42 in *cgef-1(gk261), unc-84(n369)* double mutant L1 larvae significantly enhanced the P-cell nuclear migration defects of the double mutant alone (Fig. 3C,D). Because *cgef-1(gk261)* is a predicted null, this result suggests that CGEF-1 and CDC-42 have partially independent roles, and that other RhoGTPases or GEFs may function during P-cell nuclear migration.

To test the roles of other small RhoGTPases that might function downstream of *cgef-1*, we expressed constitutively active *cdc-42*, *rho-1*, *mig-2* or *ced-10* (Alan et al., 2013; Gujar et al., 2019; Norris et al., 2014) to see whether they suppressed the nuclear migration defects of *cgef-1(yc3), unc-84(n369)* double mutants. When constitutively active *cdc-42(G12V)* was expressed from an extrachromosomal array under the control of the P-cell-specific *hlh-3* promoter, it was able to partially rescue the nuclear migration defect of *cgef-1(yc3), unc-84(n369)* double mutants (Fig. 4A,B). Although it was not a complete suppression, this result is consistent with the hypothesis that *cdc-42* is downstream of and activated by

Development (2023) 150, dev202115. doi:10.1242/dev.202115

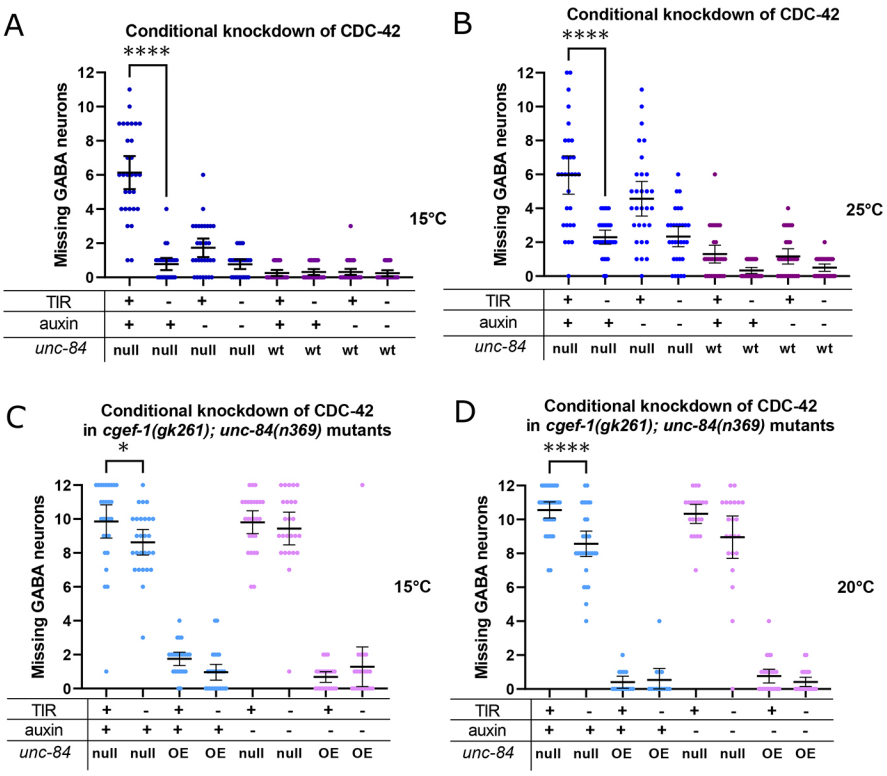

Fig. 3. CDC-42 contributes to P-cell nuclear migration. (A,B) An auxin inducible degradation (AID) system was used to knock down CDC-42 in P cells at 15°C (A) and 25°C (B). *degron::GFP11::cdc-42; unc-84(n369), oxIs12(unc-47::gfp); ycEx266(Pmyo-2::mCherry;phlh-3::TIR-1::mRuby)*, shown with blue dots, and *degron::GFP11::cdc-42; oxIs12(unc-47::gfp); ycEx266(Pmyo-2::mCherry;phlh-3::TIR-1::mRuby)*, shown with purple dots, were treated with auxin during P-cell nuclear migration. The *y*-axis shows the number of missing GABA neurons. (C,D) AID was used to knock down CDC-42 in P cells of *degron::GFP11::cdc-42*; *unc-84(n369), cgef-1(gk261), oxIs12(unc-47::gfp); ycEx300(odr-1::gfp, WRM0617cH07); ycEx266(Pmyo-2::mCherry;phlh-3::TIR-1::mRuby)* mutants at 15°C (C) and at 20°C (D). Light-blue dots indicate strains that were exposed to auxin; pink dots indicate strains that were not exposed to auxin. For all the graphs, 'OE' and 'null' for *unc-84* indicates *unc-84(n369)* null mutation with expression of the *unc-84* rescue array [*ycEx60(odr-1::rfp, WRM0617cH07)*] and no expression of the rescue array, respectively. wt indicates no *unc-84(n369)* mutation. All error bars are 95% confidence intervals and all statistical analysis was carried out using an unpaired, two-tailed Student's *t*-test. **P*<0.05, *****P*<0.0001.

cgef-1. However, when constitutively active *rho-1(G14V)*, *mig-2(G16V)* or *ced-10(G12V)* were expressed in P cells, we did not observe rescue of nuclear migration defects in *cgef-1(yc3), unc-84(n369)* mutants. Instead, we observed an enhancement of P-cell nuclear migration defects when Rac family members *mig-1(G16V)* or *ced-10(G12V)* were overexpressed in *cgef-1(yc3), unc-84(n369)* mutants (Fig. 4C-E), consistent with previous findings that Rac functions during P-cell migration (Spencer et al., 2001). In summary, our data suggest that CGEF-1 activates CDC-42 during P-cell nuclear migration.

Branched actin and actin-myosin networks contribute to P-cell nuclear migration

Although CDC-42 works in nuclear migration, it is not clear how it functions. CDC-42 regulates many downstream effectors. Here, we tested potential CDC-42 effectors involved in cell polarity (PAR-6 and PKC-3), actin networks (ARX-3 of the Arp2/3 complex) and actomyosin contractions (NMY-2) to determine their necessity for P-cell nuclear migration.

CDC-42 activates PAR-6 and PKC-3 during polarization events in early embryogenesis (Aceto et al., 2006; Gotta et al., 2001; Wang et al., 2017) and regulates non-centrosomal microtubule arrays in the larval epidermal epithelium (Castiglioni et al., 2020). We therefore hypothesized that CDC-42 functions through PAR-6 and PKC-3 during P-cell nuclear migration. We used the AID system to knock down PAR-6 and PKC-3 in P cells during nuclear migration (Castiglioni et al., 2020). Degradation of PAR-6 slightly enhanced the *unc-84(n369)* nuclear migration defect at 15°C but not at 20°C (Fig. 5A,B). However, this defect was mild compared with degrading CDC-42 in *unc-84(n369)* mutants. Furthermore, the degradation of PKC-3 did not significantly enhance the nuclear migration defect of *unc-84(n369)* (Fig. 5C,D). A caveat to this experiment is that we do not know how efficient AID of PKC-3 was, although this construct has been successfully used in other tissues (Castiglioni et al., 2020). Together, these data suggest that PAR-6 plays only a minor role during P-cell nuclear migration and that CDC-42 is functioning through an alternative pathway.

A major function performed by CDC-42 is the regulation of the assembly and dynamics of actin networks (Carlier et al., 1999; Ma et al., 1998; Rohatgi et al., 1999). To test the hypothesis that branched-actin networks function during P-cell nuclear migration, we used the AID system to degrade a component of the Arp2/3 complex. ARX-3, the *C. elegans* homolog of mammalian Arp3, is one of the seven subunits that make up the ARP2/3 complex (Sawa et al., 2003). Degradation of ARX-3 in L1 larvae at the time of P-cell nuclear migration had no defect on its own, again supporting the hypothesis that the LINC complex pathway is sufficient to move P-cell nuclei (Fig. 6A,B). However, degrading ARX-3 significantly enhanced the *unc-84(n369)* nuclear migration defect (Fig. 6A,B). Thus, we conclude that the Arp2/3 complex contributes to the movement of P-cell nuclei in the absence of LINC complexes.

We next hypothesized that myosin may be working with actin networks to exert pushing or pulling forces on P-cell nuclei. To test this hypothesis, we used the AID system by adding a degron tag onto the N terminus of the non-muscle myosin heavy chain (*nmy-2*) gene. Degradation of NMY-2 in an *unc-84(n369)* background resulted in a significantly worse nuclear-migration defect than the *unc-84(n369)* single mutant larvae (Fig. 6C-E). Therefore, CDC-42, ARX-3 and NMY-2 each contribute to migrate P-cell nuclei in the absence of LINC complexes.

DISCUSSION

Our findings presented here support the hypothesis that two parallel pathways facilitate P-cell nuclear migration: a LINC complex-dependent pathway and an actin-dependent pathway (Fig. 7). For the LINC complex pathway, the SUN protein UNC-84 spans the inner nuclear membrane and interacts with the KASH protein UNC-83 in the outer nuclear membrane. The cytoplasmic domain of

Development (2023) 150, dev202115. doi:10.1242/dev.202115

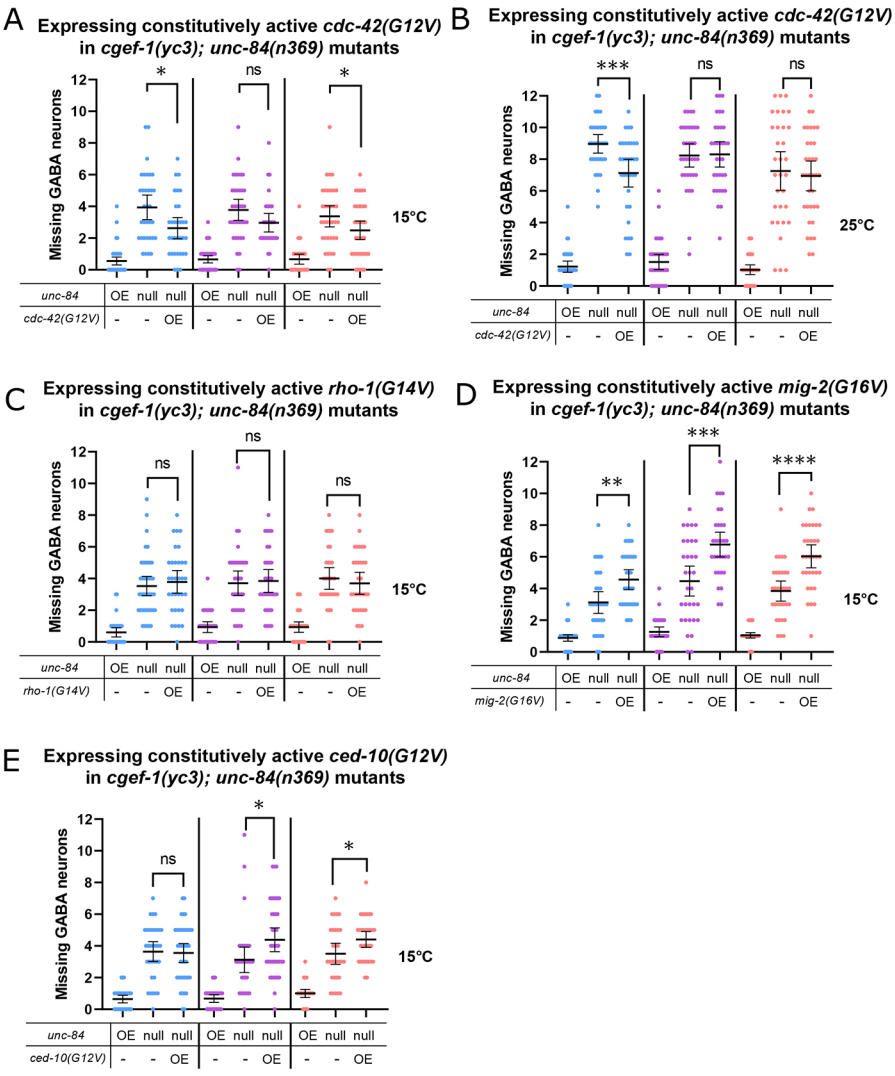

Fig. 4. CGEF-1 likely activates CDC-42 during P-cell nuclear migration. (A,B) A *phlh-3::2xHA::cdc-42(G12V); odr-1::gfp* construct was expressed in *unc-84(n369);cgef-1(yc3);oxIs12(unc-47::gfp); ycEx60(odr-1::rfp,WRM0617cH07)* in three independent lines, as indicated by the different colors. Worms were grown at 15°C (A) and 25°C (B), and assayed for P-cell nuclear migration. The *y*-axis shows the number of missing GABA neurons. (C-E) *phlh-3::2xHA::rho-1(G14V); odr-1::gfp* (C), *phlh-3::2xHA::mig-2(G16V); odr-1::gfp* (D) and *phlh-3::2xHA::ced-10(G12V); odr-1::gfp* (E) constructs were expressed in *unc-84(n369);cgef-1(yc3);oxIs12(unc-47::gfp);ycEx60(odr-1::rfp, WRM0617cH07)* in three independent lines, as indicated by the different colors. Worms were grown at 15°C and assayed for P-cell nuclear migration. The *y*-axis shows the number of missing GABA neurons. For all the graphs, OE and null for *unc-84* indicate expression of the *unc-84* rescue array [*ycEx60(odr-1::rfp,WRM0617cH07)*] and no expression of the rescue array, respectively. OE for the other transgene indicates overexpression of the indicated transgene. All error bars are 95% confidence intervals and all statistical analysis was carried out using an unpaired, two-tailed Student's *t*-test. **P*<0.05, ***P*<0.01, ****P*<0.001, *****P*<0.0001.

UNC-83 then interacts with microtubule motors kinesin 1 and dynein (Fridolfsson et al., 2010; Fridolfsson and Starr, 2010; Meyerzon et al., 2009). In P-cell nuclear migration, UNC-83 specifically recruits dynein to the nuclear envelope where it is the main motor protein that pulls nuclei towards the minus ends of microtubules (Bone et al., 2016; Ho et al., 2018).

Here, we have found that an actin-dependent pathway contributes to P-cell nuclear migration in the absence of the LINC complex pathway. In our model, CGEF-1D is a GEF, which activates the small GTPase CDC-42 during P-cell nuclear migration. CDC-42 then activates the Arp2/3 complex to nucleate branched actin. TOCA-1 and WAVE/WASP likely also work at the level of CDC-42 and Arp2/3 in this pathway (Chang et al., 2013; Giuliani et al., 2009; Raduwan et al., 2020). Once Arp2/3 nucleates actin, other proteins organize actin into networks. Although it would be ideal to genetically test whether CDC-42 and ARX-3 are in the same pathway by simultaneously knocking them both out, this would be a difficult experiment to interpret as the AID system only partially knocks down the proteins. We found that NMY-2 also plays a role in the absence of the LINC complex-dependent pathway. One hypothesis is that NMY-2 provides forces to contract actin networks during nuclear migration. Although it is known that CDC-42 can indirectly regulate NMY-2 (Gally et al., 2009; Kumfer et al., 2010; Raduwan et al., 2020; Ramesh et al., 1997; Rohatgi et al., 1999, 2000; Watson et al., 2017), further studies will need to be carried out to determine whether and how CDC-42 regulates NMY-2 in this context or even whether NMY-2 and CDC-42 are in the same or independent pathways. Further studies are also needed to describe the actin network in mutant backgrounds. There is an extensive actin network in wild-type P cells (Bone et al., 2016) but technical difficulties associated with the small size of P cells and their propensity to arrest their development, when under the mechanical pressure caused by their compression with a cover slip during imaging, have prevented us from analyzing potentially subtle defects in the actin network in mutant backgrounds.

We conclude that the actin-dependent pathway(s) is(are) important during a narrow window of development in mid-L1 when P-cell nuclei migrate. P cells divide within 1 h of nuclear migration to the ventral cord to form Pn.p daughters, which develop into hypodermal and vulval cells, and Pn.a daughters, which are neuroblasts (Sulston and Horvitz, 1977). Our enhancer mutant lines were isolated in a primary screen for Egl animals due to defects in the vulval lineages and a secondary screen where we counted GFP-positive GABA neurons (Chang et al., 2013). *cgef-1(yc3)* and *cgef-1(yc21)* disrupt both vulval and neuronal lineages, suggesting that the defect occurs before the division of Pn cells to Pn.p and Pn.a. Additionally, in *cgef-1(yc3)* or *cgef-1(yc21)* larvae, there were always the normal number of six P cells present on each lateral side

Development (2023) 150, dev202115. doi:10.1242/dev.202115

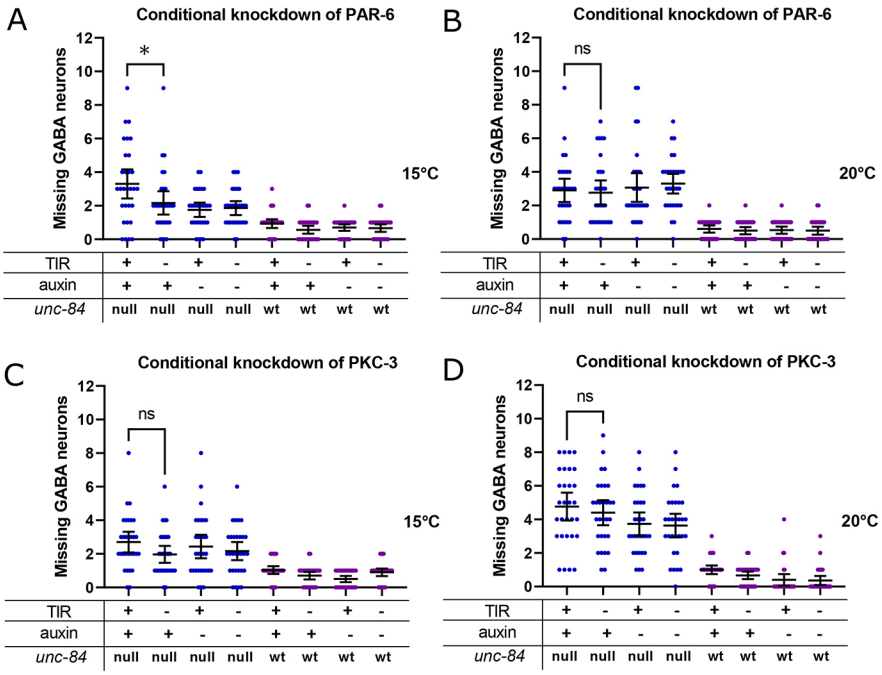

Fig. 5. PAR-6 and PKC-3 are not involved in P-cell nuclear migration. (A,B) An auxin inducible degradation (AID) system was used to knock down PAR-6 in P cells at 15°C (A) and 20°C (B). *par-6::degron::egfp; unc-84(n369), oxIs12(unc-47::gfp); ycEx266(Pmyo-2::mCherry;phlh-3::TIR-1::mRuby)*, shown with blue dots, and *par-6::degron::egfp; oxIs12(unc-47::gfp); ycEx266(Pmyo-2::mCherry;phlh-3::TIR-1::mRuby)*, shown with purple dots, were treated with auxin during P-cell nuclear migration. The *y*-axis shows the number of missing GABA neurons. (C,D) AID was used to knock down PKC-3 in P cells at 15°C (C) and 20°C (D). *egfp::degron::pkc-3; unc-84(n369), oxIs12(unc-47::gfp); ycEx266(Pmyo-2::mCherry;phlh-3::TIR-1::mRuby)*, shown with blue dots, and *egfp::degron::pkc-3; oxIs12(unc-47::gfp); ycEx266(Pmyo-2::mCherry;phlh-3::TIR-1::mRuby)*, shown with purple dots, were treated with auxin during P-cell nuclear migration. The *y*-axis shows the number of missing GABA neurons. For all the graphs, OE and null for *unc-84* indicate *unc-84(n369)* null mutation with expression of the *unc-84* rescue array [*ycEx60(odr-1::rfp, WRM0617cH07)*] and no expression of the rescue array, respectively. wt indicates no *unc-84(n369)* mutation. All error bars are 95% confidence intervals and all statistical analysis was carried out using an unpaired, two-tailed Student's *t*-test. **P*<0.05.

of an embryo or early L1 larva, and these P cells developed normally, narrowing as in wild type until just before nuclear migration (Chang et al., 2013). Thus, the crucial window for *cgef-1* function is in mid L1, after P cells narrow and before they divide in the ventral cord, which overlaps with the temporal window of P-cell nuclear migration.

Although our genetic findings implicate actin networks in nuclear migration, it is still not clear where in the cell that actin- and/or actomyosin-specific structures function to move nuclei. One possibility is that branched actin could be localized at the leading edge of the nucleus to deform it as it enters the constriction. This would be analogous to nuclei in mouse dendritic cells induced to migrate through fabricated constrictions (Thiam et al., 2016). Alternatively, actomyosin contractions could localize to the back of P-cell nuclei to provide a pushing force in the direction of migration. In migrating mammalian neurons, actomyosin contraction behind the nucleus pushes it forward and into constricted spaces (Tsai et al., 2007). In support of this model, there are thick actin cables along the direction of migration and some cells have actin rings on the lateral side of the cell near the trailing end of the nucleus during P-cell nuclear migration (Bone et al., 2016). Actomyosin contractions also provide the force that is needed for dendritic cells to migrate through confined environments with myosin enrichment at the cell rear during contraction (Barbier et al., 2019; Lämmermann et al., 2008). Future studies are required to better understand where in the cell actin-dependent pathways function during nuclear movements.

One advantage of *C. elegans* P cells as a model is that the formation of cellular protrusions, often associated with cell migrations, can be genetically separated from nuclear migrations through constricted spaces. During embryonic development, hypodermal P cells extend cytoplasmic protrusions from the lateral side of the embryo; these protrusions meet at the ventral midline to cover up the endoderm during embryonic ventral enclosure (Williams-Masson et al., 1997). Later in larval development, P-cell nuclei migrate through constrictions from lateral to ventral positions, as described above (Sulston and Horvitz, 1977). Different Rho-family GTPases function at different stages of P-cell development. Unlike in LINC complex or *cdc-42* mutants described in this article, P-cell nuclei in *rho-1* and *ced-10; mig-2* (Rac) mutants remain at their lateral starting points, retract their cytoplasm into the lateral region, remain alive, and form ectopic GABA neurons and pseudovulvae in the lateral side of the animal (Spencer et al., 2001).

Finally, even in the worst phenotypes reported here, when both the LINC complex-dependent and actin-dependent pathways were knocked out, many P-cell nuclei still successfully migrated, suggesting there are other pathways yet to be elucidated that need to be examined in future studies. For example, what role might the nuclear lamina and peripheral heterochromatin play in maintaining P-cell nuclear integrity and compression during their migration? Moreover, how is the extracellular matrix remodeled to provide sufficient space for P-cell nuclear migration to occur? We know that the fibrous organelles are removed immediately before P-cell nuclear migration (Bone et al., 2016), but determining how wide the constriction that P-cell nuclei migrate through will require the use of correlative light and electron microscopy. P cells will continue to be a valuable model for studying nuclear migrations through constricted spaces in development.

MATERIALS AND METHODS

Whole-genome sequencing of strains from the *enhancer of the nuclear migration defect of unc-84* screen

Strains carrying the *yc3*, *yc15*, *yc16*, *yc18*, *yc20* and *yc21* alleles were isolated from a previously described chemical mutagenesis screen for *enhancers of the nuclear migration defect of unc-84* (*emu*) (Chang et al., 2013). We collected genomic DNA from each homozygous mutant strain for whole-genome sequencing to identify candidate lesions underlying the nuclear migration phenotypes. Genomic DNA preps were made with the Qiagen DNeasy Blood and Tissue kit as previously described (Herrera and Starr, 2018). Genomic DNA was fragmented and made into libraries for Illumina HiSeq2500 sequencing by the Functional Genomics Laboratory at UC Berkeley. RAPID Sequencing generated 150 bp PE reads. We processed raw reads using the default settings of the CloudMap pipeline for Galaxy

Development (2023) 150, dev202115. doi:10.1242/dev.202115

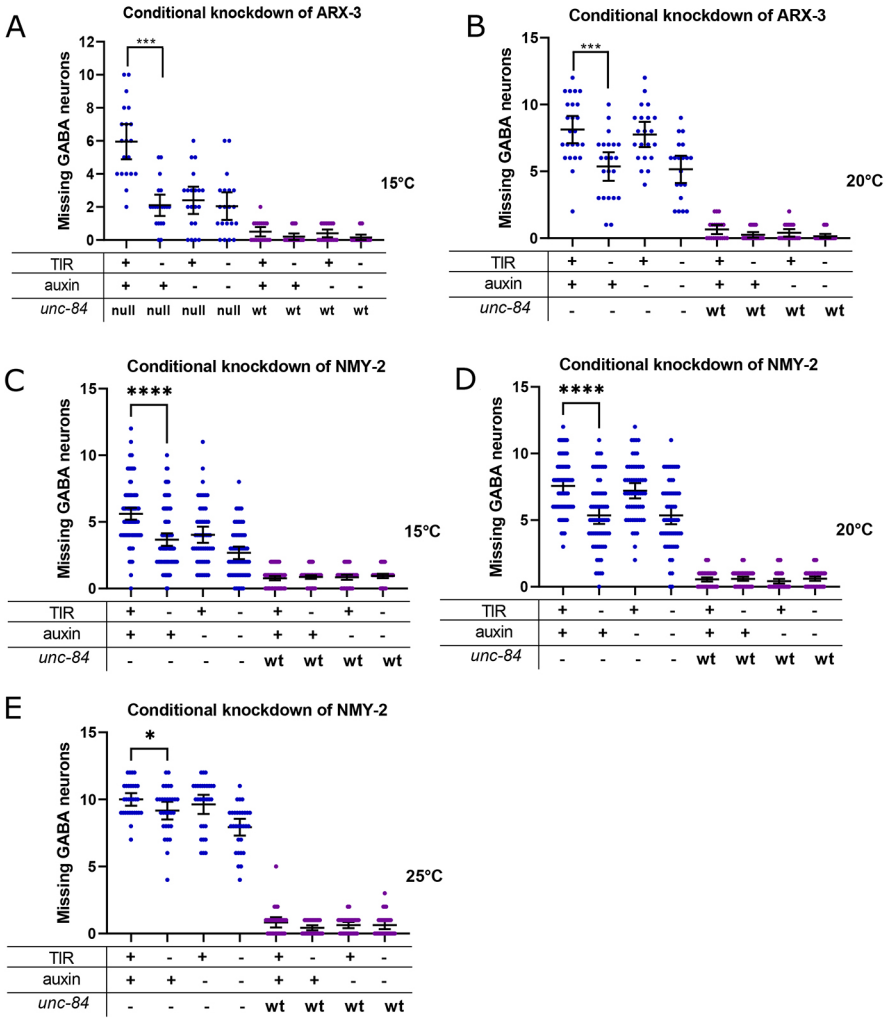

Fig. 6. Branched actin and actin-myosin contractions are involved in P-cell nuclear migration. (A,B) An auxin inducible degradation (AID) system was used to knock down ARX-3 in P cells at 15°C (A) or 20°C (B). *degron::arx-3; unc-84(n369), oxIs12(unc-47::gfp); ycEx253(odr-1::rfp; phlh-3::TIR-1::mRuby)*, shown with blue dots, and *degron::arx-3; oxIs12(unc-47::gfp); ycEx253(odr-1::rfp;phlh-3::TIR-1::mRuby)*, shown with purple dots, were treated with auxin during P-cell nuclear migration. The *y*-axis shows the number of missing GABA neurons. (C-E) AID system used to knock down NMY-2 in P cells at 15°C (C), 20°C (D) and 25°C (E). *degron::GFP11::nmy-2; unc-84(n369), oxIs12(unc-47::gfp); ycEx266(Pmyo-2::mCherry; phlh-3::TIR-1::mRuby)*, shown with blue dots, and *degron::GFP11::nmy-2; oxIs12(unc-47::gfp); ycEx266(Pmyo-2::mCherry;phlh-3::TIR-1::mRuby)*, shown with purple dots, were treated with auxin during P-cell nuclear migration. The *y*-axis shows the number of missing GABA neurons. For all the graphs, OE and null for *unc-84* indicate a *unc-84(n369)* null mutation with expression of the *unc-84* rescue array [*ycEx60(odr-1::rfp,WRM0617cH07)*] and no expression of the rescue array, respectively. wt indicates no *unc-84(n369)* mutation. All error bars are 95% confidence intervals and all statistical analysis was carried out using an unpaired, two-tailed Student's *t*-test. **P*<0.05, ****P*<0.001, *****P*<0.0001.

(Minevich et al., 2012). For each mutant line, we generated a list of variants that did not match the reference N2 genome. We excluded variants found in common between mutant lines as they were likely to be variants present in our starting strain used for the mutagenic screen (Doitsidou et al., 2016). We focused on early stop codon mutations that were present in only one or two of the six sequenced strains and identified a single nucleotide polymorphism (SNP) in the *yc3* and *yc21* strains but not the other four sequenced strains. The SNP was predicted to cause an early stop codon in *cgef-1*. No other unique mutations predicted to cause stop codons were identified in the six strains.

C. elegans strains and genetics

C. elegans animals were grown on NGM plates seeded with OP50 at their specified temperatures (Brenner, 1974). Some *C. elegans* strains used in this study were provided by the Caenorhabditis Genetics Center (CGC), which is funded by the National Institutes of Health Office of Research Infrastructure Programs (P40OD010440). The strains used in this study are described in Table S1.

For the cgef-1 RNAi experiments, clone X-2A03 from the Ahringer RNAi library (Source Bioscience) (Kamath et al., 2003) was used to create dsRNA *in vitro*, which was then injected into UD87 as described previously (Chang et al., 2013; Fire et al., 1998).

Fosmids used in the *cgef-1* rescue experiments were from the *C. elegans* Fosmid Library (Source BioScience) and were amplified in bacteria using CopyControl Induction Solution (Lucigen, CCIS125) and purified using a DNA midi prep kit (ThermoFisher Scientific, K0481). Fosmid injection mixes contained 5 ng/µl of each indicated fosmid and 100 ng/µl of *odr-1::gfp* plasmid (L'Etoile and Bargmann, 2000), and were injected into UD285.

CRISPR/Cas9 gene editing

cgef-1 isoform mutants were generated using *dpy-10* as a co-CRISPR marker (Arribere et al., 2014; Paix et al., 2015, 2017). The CRISPR injection mix was generated as described previously (Hao et al., 2021). The same guides were used to create the deletion mutations of each isoform but without the addition of the repair templates. Deletion mutations were screened by amplifying the region around the guide and PCR products that showed a smaller band size were sent for Sanger sequencing.

All crRNA and ssODN repair templates are listed in Table S2. Degron and GFP11 insertions for *cdc-42* and *nmy-2* were generated by using *zen-4(+)* as a co-CRISPR marker (Farboud et al., 2019). Single-stranded repair templates for insertions contained 50 nt homology arms (Genewiz). The CRISPR injection mix contained 0.084 µl *zen-4* crRNA (0.6 mM), 0.21 µl target gene crRNA (0.6 mM), 1.033 µl tracr (0.17 mM), 4.39 µl Cas9 (40 µM), 0.28 µl ssODN *zen-4(+)* repair template (500 ng/µl) and 4 µl ssDNA repair template (500 ng/µl). The injection mix was injected into germline of temperature-sensitive *zen-4(cle10)* mutant young adults and screened as previously described (Farboud et al., 2019).

An auxin-induced degron was inserted into the 5′ end of *arx-3*, replacing the native start codon of the gene. No linker sequence was used. The tag was inserted with a ssDNA oligo (Table 2). A *dpy-10* co-CRISPR strategy was used to identify successful injections and CRISPR repair activity (Arribere et al., 2014). The strain wLZ32[$p_{sun\text{-}1}$*::TIR-1::mRuby, Cbr-unc-119(+)*], an unnamed strain from Abby Dernburg (UC Berkeley, CA, USA) that

Development (2023) 150, dev202115. doi:10.1242/dev.202115

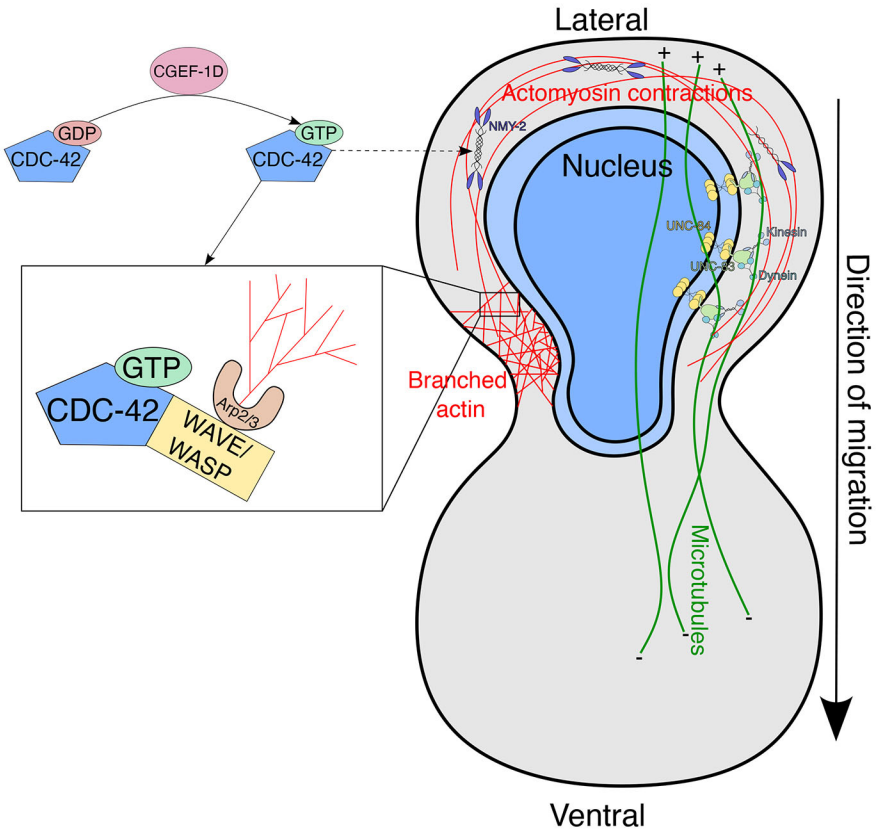

Fig. 7. Model for both pathways involved in P-cell nuclear migration. In the LINC complex-dependent pathway (right side of the cell), UNC-84 (yellow) interacts with UNC-83 (light green) at the nuclear envelope. UNC-83 interacts with both kinesin and dynein, but uses dynein as the main microtubule motor protein to pull the nucleus towards the minus ends of microtubules (green lines). The actin-based pathway is drawn on the left of the cell. CGEF-1D activates CDC-42 by exchanging the nucleotide for GTP. CDC-42 in the GTP form activates WAVE/WASP, which then activates the Arp2/3 complex to generate branched actin. CDC-42 may also be involved in indirectly activating NMY-2, which can then induce actomyosin contractions. See text for more details of our proposed model.

expresses single copy TIR1 in the germline, was used for injections. Protein Cas9 and synthetic RNA were generated by Integrated DNA Technologies.

Cloning constitutively active small Rho GTPase constructs

To generate plasmid pSL884 [$p_{hlh\text{-}3}$*::2xHA::cdc-42(G12V)::unc-54 3′UTR*], the *cdc-42(G12V)* open reading frame was amplified from pEL298 (Alan et al., 2013) with homology arms to add a 2xHA tag after the *cdc-42* start codon. To generate plasmid pSL885 [$p_{hlh\text{-}3}$*::2xHA::mig-2(G16V)::unc-54 3′UTR*], the *mig-2(G16V)* open reading frame was amplified from pEL656 (Norris et al., 2014) with homology arms to add a 2xHA tag after the *mig-2* start codon. To generate plasmid pSL886 [$p_{hlh\text{-}3}$*::2xHA::ced-10(G12V)::unc-54 3′UTR*], the *ced-10(G12V)* open reading frame was amplified from pEL777 (Norris et al., 2014) with homology arms to add a 2xHA tag after the *ced-10* start codon. To generate plasmid pSL887 [$p_{hlh\text{-}3}$*::2xHA::rho-1(G14V)::unc-54 3′UTR*], the *rho-1(G14V)* open reading frame was amplified from pEL1021 (Gujar et al., 2019) with homology arms to add a 2xHA tag after the *rho-1* start codon. The backbone of pSL830, including the promoter of *hlh-3* and the *unc-54 3′UTR* was amplified, and the HiFi DNA Assembly Cloning Kit (New England Biolabs) was used to assemble pSL884, pSL885, pSL886 and pSL887. Injection mixes containing 2 ng/µl of a plasmid encoding a constitutively active construct and 100 ng/µl of plasmid *odr-1::gfp* (L′Etoile and Bargmann, 2000) as a co-injection marker were injected into UD285. A list of plasmids for transgenic constructs are listed in Table S3.

P-cell nuclear migration assay

For the P-cell nuclear migration assays, *oxIs12[*$p_{unc\text{-}47}$*::gfp]* transgenic worms (EG1285) were used as the wild-type control (McIntire et al., 1997). *oxIs12* was used as a reporter for P-cell derived GABA neurons to assay for P-cell nuclear migration defects. L4 animals were mounted onto 2% agarose slides in 1 mM tetramisole solution. Slides were viewed using a wide-field epifluorescent Leica DM6000 microscope and a 63× Plan Apo 1.40 NA objective. UNC-47::GFP-positive GABA neurons were counted in the ventral cord. Neurons normally outside the ventral cord in the nerve ring and the most posterior neuron in the tail are not decedents of P cells and were not counted. A total of 19 GABA neurons (12 derived from P cells) was scored for each animal as previously described (Fridolfsson et al., 2018).

Synchronization and auxin assay

We synchronized *C. elegans* larvae in the mid-L1 stage at approximately the time of P-cell nuclear migration for the auxin experiments. 50-100 L4 s were picked and grown at 20°C for 24-48 h so that animals reached the adult stage. Adult animals were transferred onto a fresh NGM plate and allowed to lay eggs at 20°C for 1 h. After 1 h, the adult animals were removed, leaving synchronized embryos behind.

Conditional knockdown of proteins of interest was achieved using the auxin-inducible degradation system (Zhang et al., 2015). TIR-1 was amplified from plasmid pLZ31 (Zhang et al., 2015) (Addgene 71720) and cloned under control of the *hlh-3* promoter in pSL780 (Bone et al., 2016) with Gibson cloning (New England Biolabs) to generate pSL814. pSL814 was injected with *odr-1::rfp* to make the extrachromosomal arrays in strains UD709 and UD710. pSL814 was injected with $p_{myo\text{-}2}$*::mCherry* to make the extrachromosomal arrays in strains UD716, UD717, UD825 and UD826.

Synchronized L1 animals were washed off normal NGM plates with distilled water ∼2 h before P-cell nuclear migration began. Next, the L1 larvae were transferred to NGM+auxin plates with 1 mM 3-indoleacetic acid (IAA; Sigma, I2886) and kept in the dark. After P-cell nuclear migration was completed, the L1 larvae were washed off the NGM+auxin plates with M9 buffer and subsequently transferred to an NGM plate. For experiments performed at 15°C, embryos were left on the plates to develop for 29 h and then the resulting L1s were washed onto NGM+auxin plates and left to develop for 8 h before being washed off onto NGM plates without auxin to develop to the L4 stage. For experiments carried out at 20°C, embryos developed into L1s on NGM plates for 18 h and then placed on NGM with auxin plates for 7 h. For experiments performed at 25°C, embryos developed into L1s for 12 h and then placed on NGM with auxin plates for 6 h. These timings were determined by using the marker $p_{hlh\text{-}3}$::nls::tdTOMATO (pSL619) to visualize P-cell nuclei throughout development. Once animals

reached the L4 stage, the number of UNC-47::GFP marked GABA neurons were quantified.

To synchronize *C. elegans* for imaging, three to five plates of gravid animals were bleached, and eggs were pelleted and resuspended in M9 solution for 12-16 h at room temperature on a rocker. After starvation, L1s were plated onto NGM plates seeded with OP50 and grown at room temperature for 12 h. After 12 h, L1s were washed off the plates with M9 and mounted onto 2% agarose slides with 1 mM tetramisole solution.

Microscopy imaging

Images were taken on a Zeiss LSM 980 with Airyscan using 20× objective and the Zeiss Zen Blue software that was provided by the MCB light imaging microscopy core and by the National Institutes of Health.

Statistical analysis

Graphs of GABA neuron counts were created by using Prism (version 9). An unpaired, two-tailed Student's *t*-test was used to determine statistical significance when there was a single comparison. We used one-way ANOVA analyses with Holm-Sidak's corrections for multiple comparisons. Error bars are 95% confidence intervals.

Acknowledgements

We thank past and present members of the Starr and Luxton lab for their input on this research. We thank Zach Stevenson for help making a strain. We thank David Sherwood, Mike Boxem, Abby Dernburg and the Caenorhabditis Genetics Center (CGC), which is funded by the National Institutes of Health Office of Research Infrastructure Programs (P40OD010440), for providing strains. We thank WormBase. We thank Thomas Wilkop and the MCB Light Microscopy Imaging core for the use of a Zeiss 980 confocal microscope made available through an NIH grant S10OD026702.

Competing interests

The authors declare no competing or financial interests.

Author contributions

Conceptualization: J.H., G.W.G.L., D.A.S.; Methodology: J.H., D.A.S.; Validation: J.H., L.A.G.; Formal analysis: J.H., L.A.G.; Investigation: J.H., L.A.G.; Resources: J.H., L.A.G., D.E.L., D.A.S.; Data curation: J.H., L.A.G.; Writing - original draft: J.H., D.A.S.; Writing - review & editing: J.H., L.A.G., D.E.L., G.W.G.L., D.A.S.; Visualization: J.H.; Supervision: G.W.G.L., D.A.S.; Project administration: D.A.S.; Funding acquisition: D.A.S.

Funding

This research was funded by the National Institutes of Health (R35GM134859 to D.A.S. and R35GM128890 to D.E.L.). Open access funding provided by the University of California. Deposited in PMC for immediate release.

Data availability

All relevant data can be found within the article and its supplementary information.

Peer review history

The peer review history is available online at https://journals.biologists.com/dev/lookup/doi/10.1242/dev.202115.reviewer-comments.pdf

References

Aceto, D., Beers, M. and Kemphues, K. J. (2006). Interaction of PAR-6 with CDC-42 is required for maintenance but not establishment of PAR asymmetry in C. elegans. *Dev. Biol.* **299**, 386-397. doi:10.1016/j.ydbio.2006.08.002

Alan, J. K., Struckhoff, E. C. and Lundquist, E. A. (2013). Multiple cytoskeletal pathways and PI3K signaling mediate CDC-42-induced neuronal protrusion in C. elegans. *Small GTPases* **4**, 208-220. doi:10.4161/sgtp.26602

Arribere, J. A., Bell, R. T., Fu, B. X. H., Artiles, K. L., Hartman, P. S. and Fire, A. Z. (2014). Efficient marker-free recovery of custom genetic modifications with CRISPR/Cas9 in Caenorhabditis elegans. *Genetics* **198**, 837-846. doi:10.1534/genetics.114.169730

Barbier, L., Sáez, P. J., Attia, R., Lennon-Duménil, A.-M., Lavi, I., Piel, M. and Vargas, P. (2019). Myosin II activity is selectively needed for migration in highly confined microenvironments in mature dendritic cells. *Front. Immunol.* **10**, 747. https://www.frontiersin.org/articles/10.3389/fimmu.2019.00747.

Bell, E. S., Shah, P., Zuela-Sopilniak, N., Kim, D., Varlet, A.-A., Morival, J. L. P., Mcgregor, A. L., Isermann, P., Davidson, P. M., Elacqua, J. J. et al. (2022). Low lamin A levels enhance confined cell migration and metastatic capacity in breast cancer. *Oncogene* **41**, 4211-4230. doi:10.1038/s41388-022-02420-9

Bone, C. R. and Starr, D. A. (2016). Nuclear migration events throughout development. *J. Cell Sci.* **129**, 1951-1961. doi:10.1242/jcs.179788

Bone, C. R., Chang, Y.-T., Cain, N. E., Murphy, S. P. and Starr, D. A. (2016). Nuclei migrate through constricted spaces using microtubule motors and actin networks in C. elegans hypodermal cells. *Development* **143**, 4193-4202. doi:10.1242/dev.141192

Brenner, S. (1974). The genetics of Caenorhabditis elegans. *Genetics* **77**, 71-94. doi:10.1093/genetics/77.1.71

C. elegans Deletion Mutant Consortium. (2012). Large-scale screening for targeted knockouts in the Caenorhabditis elegans genome. *G3* **2**, 1415-1425. doi:10.1534/g3.112.003830

Carlier, M.-F., Ducruix, A. and Pantaloni, D. (1999). Signalling to actin: the Cdc42-N-WASP-Arp2/3 connection. *Chem. Biol.* **6**, R235-R240. doi:10.1016/S1074-5521(99)80107-0

Castiglioni, V. G., Pires, H. R., Rosas Bertolini, R., Riga, A., Kerver, J. and Boxem, M. (2020). Epidermal PAR-6 and PKC-3 are essential for larval development of C. elegans and organize non-centrosomal microtubules. *ELife* **9**, e62067. doi:10.7554/eLife.62067

Chan, E. and Nance, J. (2013). Mechanisms of CDC-42 activation during contact-induced cell polarization. *J. Cell Sci.* **126**, 1692-1702. doi:10.1242/jcs.124594

Chang, Y.-T., Dranow, D., Kuhn, J., Meyerzon, M., Ngo, M., Ratner, D., Warltier, K. and Starr, D. A. (2013). Toca-1 is in a novel pathway that functions in parallel with a SUN-KASH nuclear envelope bridge to move nuclei in Caenorhabditis elegans. *Genetics* **193**, 187-200. doi:10.1534/genetics.112.146589

Cox, E. A. and Hardin, J. (2004). Sticky worms: adhesion complexes in C. elegans. *J. Cell Sci.* **117**, 1885-1897. doi:10.1242/jcs.01176

Davidson, P. M., Denais, C., Bakshi, M. C. and Lammerding, J. (2014). Nuclear deformability constitutes a rate-limiting step during cell migration in 3-D environments. *Cell. Mol. Bioeng.* **7**, 293-306. doi:10.1007/s12195-014-0342-y

Davidson, P. M., Sliz, J., Isermann, P., Denais, C. and Lammerding, J. (2015). Design of a microfluidic device to quantify dynamic intra-nuclear deformation during cell migration through confining environments. *Integr. Biol.* **7**, 1534-1546. doi:10.1039/c5ib00200a

Denais, C. M., Gilbert, R. M., Isermann, P., Mcgregor, A. L., Te Lindert, M., Weigelin, B., Davidson, P. M., Friedl, P., Wolf, K. and Lammerding, J. (2016). Nuclear envelope rupture and repair during cancer cell migration. *Science* **352**, 353-358. doi:10.1126/science.aad7297

Doitsidou, M., Jarriault, S. and Poole, R. J. (2016). Next-generation sequencing-based approaches for mutation mapping and identification in Caenorhabditis elegans. *Genetics* **204**, 451-474. doi:10.1534/genetics.115.186197

Etienne-Manneville, S. (2004). Cdc42—The centre of polarity. *J. Cell Sci.* **117**, 1291-1300. doi:10.1242/jcs.01115

Farboud, B., Severson, A. F. and Meyer, B. J. (2019). Strategies for efficient genome editing using CRISPR-Cas9. *Genetics* **211**, 431-457. doi:10.1534/genetics.118.301775

Fire, A., Xu, S., Montgomery, M. K., Kostas, S. A., Driver, S. E. and Mello, C. C. (1998). Potent and specific genetic interference by double-stranded RNA in Caenorhabditis elegans. *Nature* **391**, 806-811. doi:10.1038/35888

Francis, R. and Waterston, R. H. (1991). Muscle cell attachment in Caenorhabditis elegans. *J. Cell Biol.* **114**, 465-479. doi:10.1083/jcb.114.3.465

Fricke, R., Gohl, C., Dharmalingam, E., Grevelhörster, A., Zahedi, B., Harden, N., Kessels, M., Qualmann, B. and Bogdan, S. (2009). Drosophila Cip4/Toca-1 integrates membrane trafficking and actin dynamics through WASP and SCAR/WAVE. *Curr. Biol.* **19**, 1429-1437. doi:10.1016/j.cub.2009.07.058

Fridolfsson, H. N. and Starr, D. A. (2010). Kinesin-1 and dynein at the nuclear envelope mediate the bidirectional migrations of nuclei. *J. Cell Biol.* **191**, 115-128. doi:10.1083/jcb.201004118

Fridolfsson, H. N., Ly, N., Meyerzon, M. and Starr, D. A. (2010). UNC-83 coordinates kinesin-1 and dynein activities at the nuclear envelope during nuclear migration. *Dev. Biol.* **338**, 237-250. doi:10.1016/j.ydbio.2009.12.004

Fridolfsson, H. N., Herrera, L. A., Brandt, J. N., Cain, N. E., Hermann, G. J. and Starr, D. A. (2018). Genetic analysis of nuclear migration and anchorage to study LINC complexes during development of Caenorhabditis elegans. *Methods Mol. Biol.* **1840**, 163-180. doi:10.1007/978-1-4939-8691-0_13

Friedl, P., Wolf, K. and Lammerding, J. (2011). Nuclear mechanics during cell migration. *Cell Struct. Dyn.* **23**, 55-64. doi:10.1016/j.ceb.2010.10.015

Fu, Y., Chin, L. K., Bourouina, T., Liu, A. Q. and Vandongen, A. M. J. (2012). Nuclear deformation during breast cancer cell transmigration. *Lab. Chip* **12**, 3774-3778. doi:10.1039/C2LC40477J

Gally, C., Wissler, F., Zahreddine, H., Quintin, S., Landmann, F. and Labouesse, M. (2009). Myosin II regulation during C. elegans embryonic elongation:LET-502/ROCK, MRCK-1 and PAK-1, three kinases with different roles. *Development* **136**, 3109-3119. doi:10.1242/dev.039412

Giuliani, C., Troglio, F., Bai, Z., Patel, F. B., Zucconi, A., Malabarba, M. G., Disanza, A., Stradal, T. B., Cassata, G., Confalonieri, S. et al. (2009). Requirements for F-BAR proteins TOCA-1 and TOCA-2 in actin dynamics and membrane trafficking during Caenorhabditis elegans oocyte growth and embryonic epidermal morphogenesis. *PLoS Genet.* **5**, e1000675. doi:10.1371/journal.pgen.1000675

Gotta, M., Abraham, M. C. and Ahringer, J. (2001). CDC-42 controls early cell polarity and spindle orientation in C. *elegans*. *Curr. Biol.* **11**, 482-488. doi:10.1016/S0960-9822(01)00142-7

Gujar, M. R., Stricker, A. M. and Lundquist, E. A. (2019). RHO-1 and the Rho GEF RHGF-1 interact with UNC-6/Netrin signaling to regulate growth cone protrusion and microtubule organization in Caenorhabditis elegans. *PLoS Genet.* **15**, e1007960. doi:10.1371/journal.pgen.1007960

Hall, A. (1998). Rho GTPases and the actin cytoskeleton. *Science* **279**, 509-514. doi:10.1126/science.279.5350.509

Hao, H., Kalra, S., Jameson, L. E., Guerrero, L. A., Cain, N. E., Bolivar, J. and Starr, D. A. (2021). The Nesprin-1/-2 ortholog ANC-1 regulates organelle positioning in C. elegans independently from its KASH or actin-binding domains. *ELife* **10**, e61069. doi:10.7554/eLife.61069

Herrera, L. A. and Starr, D. A. (2018). The E3 ubiquitin ligase MIB-1 is necessary to form the nuclear Halo in Caenorhabditis elegans sperm. *G3* **8**, 2465-2470. doi:10.1534/g3.118.200426

Ho, H.-Y. H., Rohatgi, R., Lebensohn, A. M., Le, M., Li, J., Gygi, S. P. and Kirschner, M. W. (2004). Toca-1 mediates Cdc42-dependent actin nucleation by activating the N-WASP-WIP complex. *Cell* **118**, 203-216. doi:10.1016/j.cell.2004.06.027

Ho, J., Valdez, V. A., Ma, L. and Starr, D. A. (2018). Characterizing Dynein's role in P-cell nuclear migration using an auxin-induced degradation system. *MicroPubl Biol.* **2018**, 10.17912/W2W96J. doi:10.17912/W2W96J

Horvitz, H. R. and Sulston, J. E. (1980). Isolation and genetic characterization of cell-lineage mutants of the nematode Caenorhabditis elegans. *Genetics* **96**, 435-454. doi:10.1093/genetics/96.2.435

Kalukula, Y., Stephens, A. D., Lammerding, J. and Gabriele, S. (2022). Mechanics and functional consequences of nuclear deformations. *Nat. Rev. Mol. Cell Biol.* **23**, 583-602. doi:10.1038/s41580-022-00480-z

Kamath, R. S., Fraser, A. G., Dong, Y., Poulin, G., Durbin, R., Gotta, M., Kanapin, A., Le Bot, N., Moreno, S., Sohrmann, M. et al. (2003). Systematic functional analysis of the Caenorhabditis elegans genome using RNAi. *Nature* **421**, 231-237. doi:10.1038/nature01278

Kengaku, M. (2018). Cytoskeletal control of nuclear migration in neurons and non-neuronal cells. *Proc. Jpn Acad. Ser. B Phys. Biol. Sci.* **94**, 337-349. doi:10.2183/pjab.94.022

Kumfer, K. T., Cook, S. J., Squirrell, J. M., Eliceiri, K. W., Peel, N., O'connell, K. F. and White, J. G. (2010). CGEF-1 and CHIN-1 regulate CDC-42 activity during asymmetric division in the Caenorhabditis elegans Embryo. *Mol. Biol. Cell* **21**, 266-277. doi:10.1091/mbc.e09-01-0060

Lämmermann, T., Bader, B. L., Monkley, S. J., Worbs, T., Wedlich-Söldner, R., Hirsch, K., Keller, M., Förster, R., Critchley, D. R., Fässler, R. et al. (2008). Rapid leukocyte migration by integrin-independent flowing and squeezing. *Nature* **453**, 51-55. doi:10.1038/nature06887

L'Etoile, N. D. and Bargmann, C. I. (2000). Olfaction and odor discrimination are mediated by the C. elegans Guanylyl Cyclase ODR-1. *Neuron* **25**, 575-586. doi:10.1016/S0896-6273(00)81061-2

Liu, J., Zhang, X., Cheng, Y. and Cao, X. (2021). Dendritic cell migration in inflammation and immunity. *Cell. Mol. Immunol.* **18**, 2461-2471. doi:10.1038/s41423-021-00726-4

Ma, L., Rohatgi, R. and Kirschner, M. W. (1998). The Arp2/3 complex mediates actin polymerization induced by the small GTP-binding protein Cdc42. *Proc. Natl Acad. Sci. USA* **95**, 15362-15367. doi:10.1073/pnas.95.26.15362

Malone, C. J., Fixsen, W. D., Horvitz, H. R. and Han, M. (1999). UNC-84 localizes to the nuclear envelope and is required for nuclear migration and anchoring during C. elegans development. *Development* **126**, 3171-3181. doi:10.1242/dev.126.14.3171

Mcgee, M. D., Rillo, R., Anderson, A. S. and Starr, D. A. (2006). UNC-83 is a KASH protein required for nuclear migration and is recruited to the outer nuclear membrane by a physical interaction with the SUN protein UNC-84. *Mol. Biol. Cell* **17**, 1790-1801. doi:10.1091/mbc.e05-09-0894

Mcintire, S. L., Reimer, R. J., Schuske, K., Edwards, R. H. and Jorgensen, E. M. (1997). Identification and characterization of the vesicular GABA transporter. *Nature* **389**, 870-876. doi:10.1038/39908

Meyerzon, M., Fridolfsson, H. N., Ly, N., Mcnally, F. J. and Starr, D. A. (2009). UNC-83 is a nuclear-specific cargo adaptor for kinesin-1-mediated nuclear migration. *Development* **136**, 2725-2733. doi:10.1242/dev.038596

Minevich, G., Park, D. S., Blankenberg, D., Poole, R. J. and Hobert, O. (2012). CloudMap: a cloud-based pipeline for analysis of mutant genome sequences. *Genetics* **192**, 1249-1269. doi:10.1534/genetics.112.144204

Norris, A. D., Sundararajan, L., Morgan, D. E., Roberts, Z. J. and Lundquist, E. A. (2014). The UNC-6/Netrin receptors UNC-40/DCC and UNC-5 inhibit growth cone filopodial protrusion via UNC-73/Trio, Rac-like GTPases and UNC-33/CRMP. *Development* **141**, 4395-4405. doi:10.1242/dev.110437

Paix, A., Folkmann, A., Rasoloson, D. and Seydoux, G. (2015). High efficiency, homology-directed genome editing in Caenorhabditis elegans using CRISPR-Cas9 ribonucleoprotein complexes. *Genetics* **201**, 47-54. doi:10.1534/genetics.115.179382

Paix, A., Folkmann, A. and Seydoux, G. (2017). Precision genome editing using CRISPR-Cas9 and linear repair templates in C. elegans. *Methods* **121-122**, 86-93. doi:10.1016/j.ymeth.2017.03.023

Raab, M., Gentili, M., De Belly, H., Thiam, H.-R., Vargas, P., Jimenez, A. J., Lautenschlaeger, F., Voituriez, R., Lennon-Duménil, A.-M., Manel, N. et al. (2016). ESCRT III repairs nuclear envelope ruptures during cell migration to limit DNA damage and cell death. *Science* **352**, 359-362. doi:10.1126/science.aad7611

Raduwan, H., Sasidharan, S., Burgos, L. C., Wallace, A. G. and Soto, M. C. (2020). RhoGAP RGA-8 supports morphogenesis in C. elegans by polarizing epithelia. *Biol. Open* **9**, bio056911. doi:10.1242/bio.056911

Ramesh, N., Antón, I. M., Hartwig, J. H. and Geha, R. S. (1997). WIP, a protein associated with Wiskott–Aldrich syndrome protein, induces actin polymerization and redistribution in lymphoidcells. *Proc. Natl. Acad. Sci. USA* **94**, 14671-14676. doi:10.1073/pnas.94.26.14671

Reiner, D. J. and Lundquist, E. A. (2018). Small GTPases. *WormBook* **2018**, 1-65. doi:10.1895/wormbook.1.67.2

Renkawitz, J., Kopf, A., Stopp, J., De Vries, I., Driscoll, M. K., Merrin, J., Hauschild, R., Welf, E. S., Danuser, G., Fiolka, R. et al. (2019). Nuclear positioning facilitates amoeboid migration along the path of least resistance. *Nature* **568**, 546-550. doi:10.1038/s41586-019-1087-5

Rohatgi, R., Ma, L., Miki, H., Lopez, M., Kirchhausen, T., Takenawa, T. and Kirschner, M. W. (1999). The interaction between N-WASP and the Arp2/3 complex links Cdc42-dependent signals to actin assembly. *Cell* **97**, 221-231. doi:10.1016/S0092-8674(00)80732-1

Rohatgi, R., Ho, H. H. and Kirschner, M. W. (2000). Mechanism of N-Wasp activation by Cdc42 and phosphatidylinositol 4,5-bisphosphate. *J. Cell Biol.* **150**, 1299-1310. doi:10.1083/jcb.150.6.1299

Rossman, K. L., Der, C. J. and Sondek, J. (2005). GEF means go: turning on RHO GTPases with guanine nucleotide-exchange factors. *Nat. Rev. Mol. Cell Biol.* **6**, 167-180. doi:10.1038/nrm1587

Salvermoser, M., Begandt, D., Alon, R. and Walzog, B. (2018). Nuclear deformation during neutrophil migration at sites of inflammation. *Front. Immunol.* **9**, 2680-2680. doi:10.3389/fimmu.2018.02680

Sawa, M., Suetsugu, S., Sugimoto, A., Miki, H., Yamamoto, M. and Takenawa, T. (2003). Essential role of the C. elegans Arp2/3 complex in cell migration during ventral enclosure. *J. Cell Sci.* **116**, 1505-1518. doi:10.1242/jcs.00362

Schmidt, A. and Hall, A. (2002). Guanine nucleotide exchange factors for Rho GTPases: turning on the switch. *Genes Dev.* **16**, 1587-1609. doi:10.1101/gad.1003302

Spencer, A. G., Orita, S., Malone, C. J. and Han, M. (2001). A RHO GTPase-mediated pathway is required during P cell migration in Caenorhabditis elegans. *Proc. Natl Acad. Sci. USA* **98**, 13132-13137. doi:10.1073/pnas.241504098

Starr, D. A. and Fridolfsson, H. N. (2010). Interactions between nuclei and the cytoskeleton are mediated by SUN-KASH nuclear-envelope bridges. *Annu. Rev. Cell Dev. Biol.* **26**, 421-444. doi:10.1146/annurev-cellbio-100109-104037

Starr, D. A., Hermann, G. J., Malone, C. J., Fixsen, W., Priess, J. R., Horvitz, H. R. and Han, M. (2001). Unc-83 encodes a novel component of the nuclear envelope and is essential for proper nuclear migration. *Development* **128**, 5039-5050. doi:10.1242/dev.128.24.5039

Stephens, A. D., Liu, P. Z., Banigan, E. J., Almassalha, L. M., Backman, V., Adam, S. A., Goldman, R. D. and Marko, J. F. (2018). Chromatin histone modifications and rigidity affect nuclear morphology independent of lamins. *Mol. Biol. Cell* **29**, 220-233. doi:10.1091/mbc.E17-06-0410

Sulston, J. E. and Horvitz, H. R. (1977). Post-embryonic cell lineages of the nematode, Caenorhabditis elegans. *Dev. Biol.* **56**, 110-156. doi:10.1016/0012-1606(77)90158-0

Sulston, J. E. and Horvitz, H. R. (1981). Abnormal cell lineages in mutants of the nematode Caenorhabditis elegans. *Dev. Biol.* **82**, 41-55. doi:10.1016/0012-1606(81)90427-9

Swift, J., Ivanovska, I. L., Buxboim, A., Harada, T., Dingal, P. C. D. P., Pinter, J., Pajerowski, J. D., Spinler, K. R., Shin, J.-W., Tewari, M. et al. (2013). Nuclear Lamin-A scales with tissue stiffness and enhances matrix-directed differentiation. *Science* **341**, 1240104. doi:10.1126/science.1240104

Thiam, H.-R., Vargas, P., Carpi, N., Crespo, C. L., Raab, M., Terriac, E., King, M. C., Jacobelli, J., Alberts, A. S., Stradal, T. et al. (2016). Perinuclear Arp2/3-driven actin polymerization enables nuclear deformation to facilitate cell migration through complex environments. *Nat. Commun.* **7**, 10997. doi:10.1038/ncomms10997

Tsai, J.-W., Bremner, K. H. and Vallee, R. B. (2007). Dual subcellular roles for LIS1 and dynein in radial neuronal migration in live brain tissue. *Nat. Neurosci.* **10**, 970-979. doi:10.1038/nn1934

Wang, S.-C., Low, T. Y. F., Nishimura, Y., Gole, L., Yu, W. and Motegi, F. (2017). Cortical forces and CDC-42 control clustering of PAR proteins for Caenorhabditis elegans embryonic polarization. *Nat. Cell Biol.* **19**, 988-995. doi:10.1038/ncb3577

Watson, J. R., Owen, D. and Mott, H. R. (2017). Cdc42 in actin dynamics: an ordered pathway governed by complex equilibria and directional effector handover. *Small GTPases* **8**, 237-244. doi:10.1080/21541248.2016.1215657

Williams-Masson, E. M., Malik, A. N. and Hardin, J. (1997). An actin-mediated two-step mechanism is required for ventral enclosure of

the C. elegans hypodermis. *Development* **124**, 2889-2901. doi:10.1242/dev.124.15.2889

Wolf, K., Te Lindert, M., Krause, M., Alexander, S., Te Riet, J., Willis, A. L., Hoffman, R. M., Figdor, C. G., Weiss, S. J. and Friedl, P. (2013). Physical limits of cell migration: control by ECM space and nuclear deformation and tuning by proteolysis and traction force. *J. Cell Biol.* **201**, 1069-1084. doi:10.1083/jcb.201210152

Zhang, L., Ward, J. D., Cheng, Z. and Dernburg, A. F. (2015). The auxin-inducible degradation (AID) system enables versatile conditional protein depletion in C. elegans. *Development* **142**, 4374-4384. doi:10.1242/dev.129635

Ziel, J. W., Matus, D. Q. and Sherwood, D. R. (2009). An expression screen for RhoGEF genes involved in C. elegans gonadogenesis. *Gene Expression Patterns* **9**, 397-403. doi:10.1016/j.gep.2009.06.005